ELSEVIER

Journal of Non-Crystalline Solids 226 (1998) 162–174

JOURNAL OF NON-CRYSTALLINE SOLIDS

X-ray absorption spectroscopic investigation of the environment of cerium in glasses based on complex cerium alkali borosilicate compositions

John G. Darab *, Hong Li, John D. Vienna

Pacific Northwest National Laboratory, [1] P.O. Box 999, Richland, WA 99352, USA

Received 6 February 1997; revised 12 January 1998

Abstract

We present the results of cerium L_{III} X-ray absorption near edge structure (XANES) studies of two series (-I and -II) of alkali boro-aluminosilicate based glasses prepared from compositions containing different amounts of CeO_2 and P_2O_5, and melted at a variety of temperatures and redox conditions. Model XANES spectra for Ce^{3+} in the glass, Ce^{4+} in the glass, and crystalline CeO_2, were used to fit the Ce L_{III} XANES spectra obtained from the glasses. This analysis allowed both the $[Ce^{4+}]/[Ce_{total}]$ ratio and the distribution of Ce environments to be determined for each glass. The $[Ce^{4+}]/[Ce_{total}]$ ratios, which varied from 0.00 to 0.58, determined independently by XANES spectroscopy were found to have a correlation, $r > 0.9$, with those previously obtained using wet chemical methods. Furthermore, using this method, these two series of glasses, which differed in the amounts of BaO, Bi_2O_3, SnO_2, and ZrO_2, had different distributions in their cerium environments. The Ce L_{III} XANES spectra obtained from series II glasses (1.0 wt% BaO, 1.0 wt% Bi_2O_3, no SnO_2, and 1.0 wt% ZrO_2) melted at 1350°C were able to be fit using only Ce^{3+}_{glass} and Ce^{4+}_{glass} environments; whereas, those from series I glasses (2.7 wt% SnO_2, no BaO or Bi_2O_3, and 5.1 wt% ZrO_2) melted at 1120°C could only be fit when an additional $Ce^{4+}_{CeO_2}$ component was included, confirming the previous assessment that the series I glasses exhibited CeO_2 related heterogeneities.

1. Introduction

Cerium containing glasses are of technical importance for a variety of reasons [1]. For example, $Na_2O–Al_2O_3–B_2O_3–SiO_2$ systems containing precipitated Ce^{4+} phases have applications in glasses and glazes requiring deep yellow coloration [1,2]. $Li_2O–MgO–SiO_2$ and related glasses containing Ce^{3+} are used as thermal neutron detectors [3]. Television glass faceplates are formulated to contain mixtures of Ce^{3+} and Ce^{4+} ions which are used to scavenge color centers generated by the electron bombardment that occurs during operation [1]. It has been suggested that cerium (Ce) may act as a non-radioactive surrogate for plutonium (Pu) that emulates its chemical and structural behavior during Pu-waste

* Corresponding author. Tel.: +1-509 375 6608; e-mail: jg_darab@pnl.gov.

[1] Pacific Northwest National Laboratory is operated for the United States Department of Energy by the Battelle Memorial Institute under contract DE-AC06-76RLO 1830.

0022-3093/98/$19.00
PII S0022-3093(98)00369-X

vitrification [4,5]. Such plutonium surrogates are required for the non-radiological laboratory-scale experiments and melter vendor evaluations associated with defense waste clean-up programs. Thus, an understanding of how the chemistry of Ce behaves with respect to Pu under a variety of vitrification conditions is required. In all the applications discussed above, it is apparent that the determination of the relative amounts of Ce^{3+} and Ce^{4+} (i.e., $[Ce^{4+}]/[Ce_{total}]$ or $[Ce^{3+}]/[Ce^{4+}]$) is an important aspect in understanding the observed properties of these glasses and in developing new glass formulations and processing routes.

One method of determining the cerium redox chemistry in glasses involves a well established wet chemical technique [2,6]. For example, the glass sample to be analyzed is dissolved in ≈ 1.5 N H_2SO_4 and titrated with 0.002 N ferrous ammonium sulfate in 1 N H_2SO_4 using ferroin as an endpoint indicator [6]. During glass dissolution but prior to titration, the $[Ce^{4+}]/[Ce_{total}]$ ratio that was inherent in the glass may change in solution due to redox couples with, for example, water. This change becomes especially important when analyzing chemically durable glasses, such as those studied here, were HF needs to be used in conjunction with H_2SO_4 to dissolve the glass. The presence of HF in solution slowly reduces Ce^{4+} to Ce^{3+} [6]. Calibration titrations on solutions made from glass samples containing no CeO_2 mixed with known amounts of Ce^{4+} are thus required to account for these changes in redox chemistry during glass dissolution.

This analysis allows the initial concentration of Ce^{4+} in the dissolved glass to be determined from the volume of titrant added. Using the calibration curve, the concentration of Ce^{4+} that was in the original glass can then be estimated. Of course, a separate determination of the total concentration of cerium in the glass must also be made to get an accurate evaluation of $[Ce^{4+}]/[Ce_{total}]$, which adds to the error in the analysis. Furthermore, for glasses containing multivalent metal ions that can couple to the Ce^{3+}/Ce^{4+} reaction (e.g., Fe^{2+}/Fe^{3+}), this technique yields ambiguous results. Since most waste glasses contain a host of transition metal and other metal cations, evaluating $[Ce^{4+}]/[Ce_{total}]$ for these glasses using this technique will most likely not be possible.

Another method of determining the cerium redox in glasses involves measuring the Ce L_{III} X-ray absorption edge using synchrotron radiation [3,7]. This technique is commonly employed for redox determinations of many elements in solids such as glasses, ceramics, and coals, without the need for dissolving the sample. Since the method is element-specific, one can in principle analyze materials of complex chemistry (nuclear waste glasses, for example). The X-ray absorption spectrum in the vicinity of the edge (X-ray absorption near edge structure or XANES) is sensitive, both in edge energy and spectral line shape, to the oxidation state, first neighbor coordination symmetry and even distant neighbor structure [7]. As will be shown below, the XANES features for Ce^{3+} and Ce^{4+} species are resolved enough to allow the determination of the $[Ce^{4+}]/[Ce_{total}]$ for a particular glass using a single measurement.

Here, we discuss the use of XANES spectroscopy in determining both the $[Ce^{4+}]/[Ce_{total}]$ ratio as well as the distribution of Ce environments in two different series of simulated plutonium waste glasses. Our goal is to independently compare and contrast the results obtained from the XANES technique with those obtained from wet chemical analysis. The glass systems were selected because neither contains Fe_2O_3, which would interfere with the wet chemical analysis.

The target base line compositions of the series I (Pu10S-I) and series II (Pu10S-II) glasses are summarized in Table 1. The nomenclature used here, i.e., Pu10S-I or -II, indicates that the glasses were developed from a nominal Pu base line waste glass composition containing 10 wt% PuO_2 (*Pu10*S-I). For the simulated (i.e., non-radioactive) glasses (Pu10*S*-I), the molar concentration of CeO_2 was kept identical to that of PuO_2 in the Pu base line waste glass. The base line glass series is designated with -I or -II and modifications to the composition or processing conditions are identified with a letter, e.g., Pu10S-Ia.

2. Experimental

2.1. Preparation of glasses

Based on the compositions listed in Table 1, glasses containing varying amounts of CeO_2, P_2O_5

Table 1
Target compositions of the simulated base line plutonium waste glasses used in this work (in wt% oxide basis)

Component	Base line glass	
	Pu10S-I	Pu10S-II
SiO_2	46.39	54.45
Al_2O_3	2.31	5.18
B_2O_3	12.14	7.27
BaO	–	1.04
Bi_2O_3	–	1.05
CeO_2	6.49	6.49
Cs_2O	0.93	1.03
Gd_2O_3	3.41	6.86
K_2O	5.22	2.07
Li_2O	4.02	2.08
Na_2O	9.21	10.39
SnO_2	2.73	–
TiO_2	2.06	1.04
ZrO_2	5.10	1.04

and graphite (see Table 2) with the remaining components proportionately adjusted were prepared. Glass batch materials were made by combining chemical reagents (SiO_2, Al_2O_3, H_3BO_3, $BaCO_3$, Bi_2O_3, CeO_2, Cs_2CO_3, Gd_2O_3, K_2CO_3, Li_2CO_3, Na_2CO_3, SnO_2, TiO_2, ZrO_2, graphite, and $NaPO_3$) in the appropriate amounts to the nearest 0.01 g using a top loading electronic balance. Each batch was then homogenized in a grinding machine (Angstrom) for 5 min. Batch sizes were of sufficient mass to yield a total of ≈ 100 g of oxide after vitrification. Using a Pt–10% Rh crucible, each glass was prepared by melting the batch material in a furnace (Deltech DT-31) at 1120 ± 2°C for Pu10S-I glasses or 1350 ± 3°C for Pu10S-II glasses for a duration of 2 to 16 h (see Table 2). Melts were conducted in air with the crucible covered by a Pt–10% Rh lid. A platinum rod was used to stir the melt midway through the time at melting temperature. The glass was then quenched by pouring onto a stainless steel plate.

The final composition of two of the prepared materials, Pu10S-If and Pu10S-IIa, were determined by measuring the elemental concentrations using inductively coupled plasma atomic emission spectroscopy (ICP-AES), see Table 3. The theoretical compositions of these same materials, assuming no volatilization during melting, can be determined from the masses of the batch chemical reagents. Considering the precision of the balance and the ≈ 100 g batch size, the relative error in the theoretical final composition ranges from approximately 0.05% to 0.10% for each component. The theoretical compositions along with their errors are also listed in Table

Table 2
Sample nomenclature, CeO_2 and P_2O_5 content in melt feed, type of reductant used, and melt temperature and duration for selected glasses

Sample	CeO_2 (wt%)	P_2O_5 (wt%)	Reductant	T_m (°C)	Time (h)
Pu10S-Ia	3.0 ± 0.01	–	–	1120 ± 2	4
Pu10S-Ic	4.5 ± 0.01	–	–	1120 ± 2	4
Pu10S-Ie[a]	6.0 ± 0.01	–	–	1120 ± 2	4
Pu10S-If	6.5 ± 0.01	–	graphite	1120 ± 2	4
Pu10S-IIa	6.5 ± 0.01	–	–	1350 ± 3	2
Pu10S-IIb	10.5 ± 0.01	–	–	1350 ± 3	4
Pu10S-IIc	15.0 ± 0.01	–	–	1350 ± 3	16
Pu10S-IIi	6.3 ± 0.01	3.3 ± 0.01	–	1350 ± 3	2
Pu10S-IIj[b]	6.2 ± 0.01	4.9 ± 0.01	–	1350 ± 3	2

[a] CeO_2 crystals were identified in this glass.
[b] Glass was opalescent.

Table 3
Theoretical and actual compositions of two simulated plutonium waste glasses studied in this work (in wt% oxide basis)

Component	Sample composition			
	Pu10S-If		Pu10S-IIa	
	Theoretical	Actual	Theoretical	Actual
SiO_2	46.39 ± 0.01	46.65 ± 3.19	54.45 ± 0.01	53.29 ± 3.65
Al_2O_3	2.31 ± 0.01	2.32 ± 0.16	5.18 ± 0.01	5.22 ± 0.36
B_2O_3	12.14 ± 0.01	11.45 ± 0.78	7.27 ± 0.01	7.11 ± 0.49
BaO	–	–	1.04 ± 0.01	0.98 ± 0.07
Bi_2O_3	–	–	1.05 ± 0.01	0.87 ± 0.06
CeO_2	6.49 ± 0.01	6.63 ± 0.45	6.49 ± 0.01	6.11 ± 0.42
Cs_2O	0.93 ± 0.01	0.94 ± 0.06	1.03 ± 0.01	0.87 ± 0.06
Gd_2O_3	3.41 ± 0.01	3.47 ± 0.24	6.86 ± 0.01	6.38 ± 0.48
K_2O	5.22 ± 0.01	5.34 ± 0.37	2.07 ± 0.01	2.13 ± 0.15
Li_2O	4.02 ± 0.01	[a]	2.08 ± 0.01	[a]
Na_2O	9.21 ± 0.01	9.37 ± 0.64	10.39 ± 0.01	10.67 ± 0.75
SnO_2	2.73 ± 0.01	2.77 ± 0.19	–	–
TiO_2	2.06 ± 0.01	2.09 ± 0.14	1.04 ± 0.01	1.05 ± 0.07
ZrO_2	5.10 ± 0.01	5.27 ± 0.36	1.04 ± 0.01	0.97 ± 0.07

Actual compositions were determined from the elemental concentrations measured by ICP-AES.
[a] The elemental concentration of Li could not be determined using ICP-AES.

3. The measured composition of the Pu10S-If sample was within experimental error of the theoretical composition for each component. Comparison between the theoretical and measured compositions for the Pu10S-IIa sample, however, indicates that Bi_2O_3 and Cs_2O exhibited approximately 10–20% loss by weight after melting the batch material, presumably due to volatilization.

2.2. XANES measurements

XANES spectra were obtained at room temperature on beam line X19A at the National Synchrotron Light Source (NSLS). The data were obtained in transmission mode using samples prepared by thinly distributing ground glass samples (−325 mesh) on cellophane tape. The beam line used a Si (111) double crystal monochromator and standard ionization detectors. For each scan, the incident and transmission X-ray intensities were recorded as a function of X-ray energy, E, allowing the absorption coefficient, μ, to be determined. Data for the near edge spectrum (i.e., XANES) was collected between 5673 eV and 5773 eV which is appropriate for the Ce L_{III} edge (5723 eV for Ce metal). Monochromator step increments were 0.2 eV between 5693 eV and 5733 eV. X-ray energies were calibrated using CeO_2 as a reference. Between three and fifteen scans were taken for each sample, depending on the strength of the signal, and averaged. For each sample, one to two scans out to 6123 eV were also obtained to determine the X-ray absorption step height. Each set of averaged XANES data was then normalized with respect to its step height.

3. Results

Glasses were considered to be homogeneous when no secondary phases were detected using optical microscopy (≈ 1 μm feature resolution) and X-ray diffraction (XRD, > 20 nm resolution of crystalline phases). Based on previous work performed on these series, samples Pu10S-Ia, Pu10S-Ic, Pu10S-If, Pu10S-IIa, Pu10S-IIb, Pu10S-IIc, and Pu10S-IIi were found to be homogeneous, as defined above. In contrast, crystals of CeO_2 were observed in sample Pu10S-Ie (see Table 2).

Sample Pu10S-IIj was opalescent, indicating that phase separation had occurred in that glass as well. The nature of this phase separation in sample Pu10S-IIj is the subject of ongoing research, but is believed to be due to the presence of excess P_2O_5 (see Table 2). Similar P_2O_5-induced phase separation was previously observed in Na_2O–CaO–Al_2O_3–B_2O_3–SiO_2 low-level waste (LLW) glass systems [8].

Fig. 1 shows the Ce L_{III} XANES obtained from a Pu10S-If sample melted with graphite, which was chemically determined to contain only Ce^{3+}. The

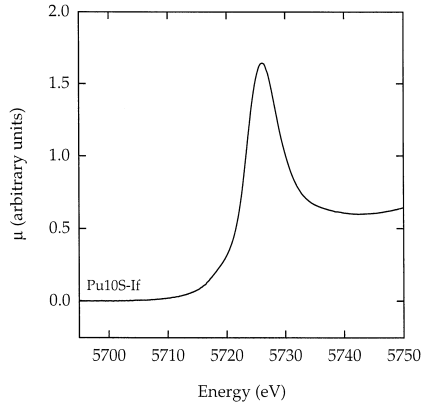

Fig. 1. Cerium L_{III} edge obtained from the Pu10S-If glass melted with graphite. Chemical analysis indicated this glass contained only Ce^{3+}.

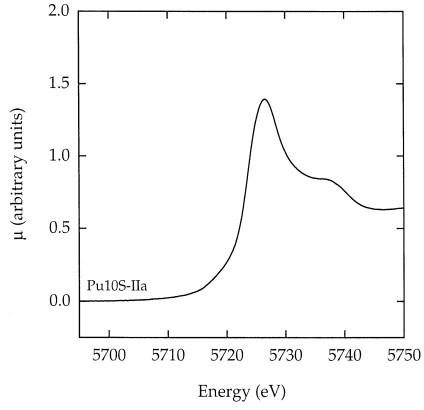

Fig. 2. Cerium L_{III} edge obtained from the Pu10S-IIa glass. Chemical analysis indicated this glass contained a mixture of Ce^{3+} and Ce^{4+} ($[Ce^{4+}]/[Ce_{total}] = 0.36$).

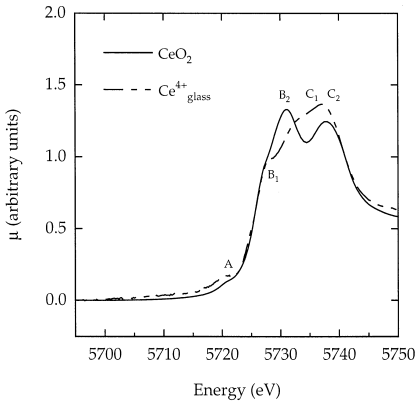

Fig. 3. Cerium L_{III} edge obtained from the CeO_2 reference material (solid line). The labels *A*, B_1, B_2, C_1, and C_2 correspond to the nomenclature used by Le Normand et al. [9] and identify different XANES features. For comparison, the dashed line represents the extracted XANES of the Ce^{4+}_{glass} environment (see text and Fig. 4).

singular intense peak at 5726 eV (5726.0 ± 0.2 eV) is characteristically observed in Ce^{3+} compounds (5725.5 eV [9], 5726.2 eV [10]).

Fig. 2 shows the Ce L_{III} XANES obtained from a Pu10S-IIa sample ($[Ce^{4+}]/[Ce_{total}] = 0.36$, determined chemically [11]). In addition to the XANES peak at 5726 eV (5726.6 ± 0.2 eV), a peak is observed at ≈ 5740 eV, which we attribute to the presence of Ce^{4+} in agreement with literature results [12,13], and which corroborates the chemical result.

As a comparison, Fig. 3 shows the Ce L_{III} XANES obtained from the CeO_2 reference material. The labels *A*, B_1, B_2, C_1, and C_2 correspond to the nomenclature used by Le Normand et al. [9] for identifying the various features in their Ce L_{III} XANES. For CeO_2 data presented in Fig. 3, these features occur at the following approximate energies (eV): 5720 (*A*), 5727 (B_1), 5731 (B_2), 5737 (C_1), and 5739 (C_2). Multiple *B* features have also been identified by Bianconi et al. [13]. Note that the *C* features (C_1 and C_2), which are not readily resolvable from each other, comprise the ≈ 5740 eV peak described above.

The Ce L_{III} XANES experimentally obtained from all the samples in the Pu10S-II and Pu10S-I series

Table 4
Results (% Ce^{4+} with respect to Ce_{total}) of chemical [11] and XANES analyses on selected glasses

Glass	CeO_2 (wt%)	Ce^{4+} (% *w/r* Ce_{total})		XANES fit (% of component)		
		Chemical	XANES	Ce^{3+}_{glass}	Ce^{4+}_{glass}	$Ce^{4+}_{CeO_2}$
Pu10S-Ia	3.0	nm	53 ± 5	47 ± 5	49 ± 5	4 ± 2
Pu10S-Ic	4.5	47 ± 6	51 ± 5	48 ± 5	38 ± 4	13 ± 3
Pu10S-Ie[a]	6.0	nm	58 ± 5	42 ± 5	35 ± 4	23 ± 3
Pu10S-If[b]	6.5	0[e]	0[f]	100	0[f]	0[f]
Pu10S-IIa	6.5	36 ± 5	28 ± 3	72 ± 3	28 ± 3	0[g]
Pu10S-IIb	10.5	29 ± 4	17 ± 3	83 ± 3	17 ± 3	0[g]
Pu10S-IIc	15.0	25 ± 4	17 ± 3	83 ± 3	17 ± 3	0[g]
Pu10S-IIi[c]	6.3	25 ± 4	18 ± 3	82 ± 3	18 ± 3	0[g]
Pu10S-IIj[c,d]	6.2	24 ± 4	15 ± 3	85 ± 3	15 ± 3	0[g]

Also included are the relative contributions of each environment (Ce^{3+}_{glass}, Ce^{4+}_{glass}, and $Ce^{4+}_{CeO_2}$) deconvoluted from the overall XANES.
[a] Undissolved CeO_2 crystals were identified in this glass.
[b] Graphite was added to the melt as a reductant.
[c] $NaPO_3$ was added to the melt feed.
[d] Glass was opalescent.
[e] The detection limit of the technique is approximately 3% Ce^{4+}. The measured relative amount of Ce^{4+} in sample Pu10S-If is thus $< 3\%$ but is reported as 0% for simplicity.
[f] The combined contribution of all Ce^{4+} environments (Ce^{4+}_{glass} and $Ce^{4+}_{CeO_2}$) to the total Ce XANES of sample Pu10S-If is reported as 0% since that gave the best fit to the data. However, inclusion of up to 2% Ce^{4+} still allowed for a reasonable (although not the best) fit to the data. The relative amount of Ce^{4+} in sample Pu10S-If determined by XANES is thus $< 2\%$ but is reported as 0% for simplicity.
[g] The contribution of the $Ce^{4+}_{CeO_2}$ environment to the total Ce XANES of sample Pu10S-If is reported as 0% since that gave the best fit to the data. However, inclusion of up to 2% $Ce^{4+}_{CeO_2}$ still allowed for a reasonable (although not the best) fit to the data. The relative amount of $Ce^{4+}_{CeO_2}$ in these samples determined by XANES is thus $< 2\%$ but is reported as 0% for simplicity.
nm = not measured.

are depicted in Fig. 5a and b, respectively (see below).

The nominal CeO_2 concentration and the relative amount of Ce^{4+} with respect to the total Ce content previously determined by chemical methods [11] are summarized in Table 4 for each glass.

4. Discussion

4.1. XANES features

A discussion concerning the ≈ 5740 eV peak observed in the Ce L_{III} XANES spectrum of the Pu10S-IIa sample (and in the other samples) is in order since this feature may be useful as an identifying and quantitative marker for the determination of the $[Ce^{4+}]/[Ce_{total}]$ ratio in glasses.

Cerium (IV) moieties (e.g., Ce–O complexes in glasses) can be described by two different ground state ionic configurations: $4f^0$ and $4f^1\underline{L}$, where $\underline{L}$ indicates a ligand O 2p hole [12]. The corresponding final ionic states resulting from the $2p \rightarrow 5d$ XANES transitions are thus $M5d^14f^0$ and $M5d^14f^1\underline{L}$, where M represents the Ce 2p hole. These two possible final electronic configurations give rise to different Coulombic interactions between the excited 5d electron, the 4f electron (for the $4f^1\underline{L}$ case), and the Ce 2p core hole. It is generally believed [9,13] that the transition to $M5d^14f^0$ gives rise to a XANES peak at ≈ 5740 eV, features C_1 and C_2 in Fig. 3, whereas that to $M5d^14f^1\underline{L}$ occurs ≈ 10 eV lower in energy (≈ 5730 eV), features B_1 and B_2. These two features are observed in the Ce L_{III} XANES spectrum of CeO_2 (Fig. 3). On this basis, the peak at ≈ 5740 eV in the XANES spectrum of the Pu10S-I and Pu10S-II glass samples (Figs. 2 and 5) were attributed to the Ce^{4+} $4f^0 \rightarrow M5d^14f^0$ transition.

It has been reported that for crystalline $CeTiO_3$ and related phases, an additional, less intense Ce L_{III} XANES peak occurs in the vicinity of ≈ 5740 eV (5738.0 eV) and has been attributed to photoelectron backscattering from the nearest oxygen neighbors arranged around Ce^{3+} in the crystalline structure [10]. For these presumed Ce^{3+} compounds, however, no discussion was given concerning the confirmed presence of a significant amount of Ce^{4+} [10], which would also give rise to a peak at ≈ 5740 eV. Although not specifically mentioned, the ≈ 5740 eV Ce L_{III} XANES peak was observed in Ce_2MoO_6 [12] as well. Since oxygen non-stoichiometry in this compound is not expected and electron paramagnetic resonance (EPR) evidence exists that indicates the presence a minor amount of Mo^{5+} (the balance being Mo^{6+}) [12], a minor amount of Ce^{4+} to maintain charge balance would seem likely, i.e., $Ce^{(3+)}_{2-x}Ce^{(4+)}_{x}Mo^{(6+)}_{1-x}Mo^{(5+)}_{x}O_6$ and would explain the presence of the observed 5740 eV peak.

For the reduced Pu10S-If sample (100% of the total cerium is Ce^{3+}), no peak at or near ≈ 5740 eV was observed in the XANES spectrum (see Fig. 1). This result gives us confidence that the Ce L_{III} XANES feature at ≈ 5740 eV observed in the other glasses studied here is not due to Ce^{3+} species, but rather from the presence of Ce^{4+} species.

4.2. Distribution of cerium environments and glass homogeneity

The solubility limit of a particular component (in this case Ce) in a glass is generally represented by a critical concentration, below which the glass is homogeneous while above it is heterogeneous or phase separated. However, the propensity of certain transition metal and rare earth ions to form supermolecular structures (e.g., oligomers, clusters, etc.) in aqueous solutions and in melts makes the difference between homogeneous and phase-separated glasses less resolved [14,15]. For example, polychromium(III) species can form in both aqueous solutions and $Na_2O–CaO–B_2O_3–Al_2O_3–SiO_2$ glasses, which represents molecular or nanometer-sized heterogeneities in otherwise homogeneous systems [15]. Likewise, reviewing the chemistry of Ce^{4+}, which is described as being similar to that of Zr^{4+} (and Hf^{4+}) [16,17], we expect similar polycerium(IV) heterogeneities to form in some glasses as well.

With these caveats in mind, we have assumed that there are three possible Ce environments in our samples. The first two include Ce^{3+}_{glass} and Ce^{4+}_{glass}, which encompass $Ce^{3+/4+}$ species that may be homogeneously incorporated into the network as well as species associated with the molecular heterogeneities mentioned above. The third type of environment is that for Ce^{4+} as separated CeO_2 and related solid solutions, $Ce^{4+}_{CeO_2}$, and may include

nanometer-sized phases as well. As will be discussed below, by assigning a model XANES spectrum to each of these Ce environments, the overall XANES spectrum obtained for a particular glass can be fitted using weighted contributions from the three environments.

4.3. XANES spectra of cerium environments

The experimental XANES spectra depicted in Figs. 1–3 would usually be analyzed by fitting the spectra using a series of functions. Blanchard et al. [3] used a cumulative Gaussian step function together with a series of Voigt functions, which account for both natural line shape (Lorentzian) and detector broadening effects (Gaussian) to fit Ce L_{III} XANES spectra obtained from Li_2O–MgO–SiO_2 and related glasses. Others reported to have fit Ce edge data in compounds using an arctangent function and one or two (for the case of Ce^{4+} compounds) Lorentzian functions, although the fits themselves were not presented [12]. The need for using up to two arctangent step functions and five Lorentzian functions when fitting Ce L_{III} XANES data has been presented [9,13].

These methods are not without their problems, however, and we have elected to rely on a more novel approach to analyzing the Ce L_{III} XANES spectra which will be discussed in detail below. However, because the analyses of XANES spectra are often performed in the manner described above, for thoroughness, we have analyzed the Ce L_{III} XANES spectra obtained from some of our samples in this way as well. The results of this analysis are summarized in Appendix A.

For our samples, up to two arctangent and seven Lorentzian functions were required to fit their XANES spectra. Such a large number of variables in the fitting procedure often results in non-unique solutions [13]. Furthermore, in comparing fits to Ce^{3+} and Ce^{4+} compounds, the functions corresponding to the B_1 and B_2 features in the two oxidation states often overlap, leaving the C feature as the only unique fingerprint of Ce^{4+} [3]. Thus, although one can determine the relative C feature (≈ 5740 eV peak) area with respect to the total area, calibration to a set of standards of known $[Ce^{4+}]/[Ce_{total}]$ is still required to get quantitative information out of the analysis.

An alternative method is to use model XANES spectra of reference compounds to fit the data obtained from the glasses and to get a direct quantitative value of $[Ce^{4+}]/[Ce_{total}]$. Here, we have used the Ce L_{III} XANES spectrum obtained from a reduced Pu10S-If sample (Fig. 1) as a model for that of Ce^{3+}_{glass}. The spectrum of CeO_2 (Fig. 3) was used as a model for the XANES of $Ce^{4+}_{CeO_2}$. A model for the Ce^{4+}_{glass} XANES, however, was not directly available since we were not able to prepare a homogeneous glass containing only Ce^{4+}.

To circumvent this impasse, two options were available. For a first approximation, the XANES of Ce^{4+}_{glass} could be assumed to be the same as that of $Ce^{4+}_{CeO_2}$. Unsuccessful attempts were made to fit the XANES data obtained from the glasses using only the Ce^{3+}_{glass} and $Ce^{4+}_{CeO_2}$ models. This failure is not surprising since the initial assumption was not necessarily valid. Even though the XANES of Ce^{4+}_{glass} and $Ce^{4+}_{CeO_2}$ may both have the same edge energy and contain the same spectral components (A, B_1, B_2, C_1, and C_2), the relative proportions of each component, and hence the overall line shape, depend on the covalent fraction of the Ce–O bonds and longer range interactions in the system [9,13], which were not expected to be the same for the two environments.

Another approach, and the one taken here, was to extract the Ce^{4+}_{glass} XANES model from the available information using several assumptions. The XANES data collected is in the form of X-ray absorption coefficient (μ) vs. energy (E). The XANES data obtained from a Pu10S-If sample (Ce^{3+}_{glass}) was systematically subtracted from that from a homogeneous Pu10S-IIa sample (mixture of Ce^{3+}_{glass} and Ce^{4+}_{glass}) obtaining a series of residue XANES spectra assuming the following relation holds: $\mu(E)_{\text{Pu10S-IIa}} = f_{\text{Pu10S-If}}\ \mu(E)_{\text{Pu10S-If}} + f_{\text{residue}}\ \mu(E)_{\text{residue}}$, where f_i is the fraction of component i that comprises the Pu10S-IIa XANES and $f_{\text{Pu10S-If}} + f_{\text{residue}} = 1$. Fig. 4 depicts the residue XANES obtained by considering that $f_{\text{Pu10S-If}}$ is 0.80, 0.72, and 0.64, the latter of which is equal to that derived from the chemical analysis ($[Ce^{4+}]/[Ce_{total}] = 0.36$).

Assuming that the correct amount of Ce^{3+}_{glass} model XANES was subtracted from the data, the Ce^{4+}_{glass}

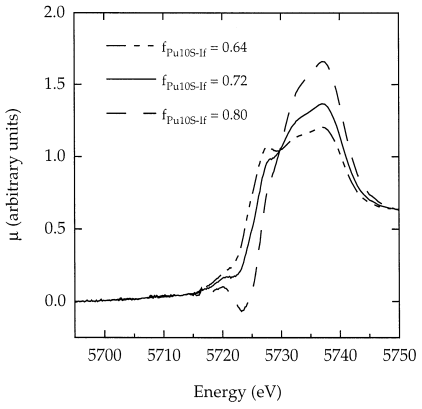

Fig. 4. Residual XANES obtained by considering that the fraction of Pu10S-If XANES that comprises the total Pu10S-IIa XANES, $f_{Pu10S-If}$, is equal to 0.80, 0.72, and 0.64 (see text). The residual labeled $f_{Pu10S-If} = 0.72$ (solid line) has been used as a model to represent the Ce^{4+}_{glass} environment and is shown in Fig. 3 for comparison with the $Ce^{4+}_{CeO_2}$ environment.

model XANES could be obtained from the residue. We have assumed that the edge energy of the Ce^{4+}_{glass} model XANES was close (within ± 1 eV) of the $Ce^{4+}_{CeO_2}$ edge energy, since the oxidation states of these two environments were the same. [2] The environments of Ce^{3+}_{glass}, Ce^{4+}_{glass}, and $Ce^{4+}_{CeO_2}$ were also assumed to be similar in all the samples studied here. This similarity allowed us to narrow the contribution of the Pu10S-If sample XANES (Ce^{3+}_{glass}) to the overall Pu10S-IIa sample XANES at $f_{Pu10S-If} = 0.72 \pm 0.03$. For $f_{Pu10S-If} = 0.72$, the residue (presumably the XANES from Ce^{4+}_{glass}) edge energy lines up precisely with that of $Ce^{4+}_{CeO_2}$. At $f_{Pu10S-If} = 0.69$ (not shown) the residue edge energy was about -1 eV from that of $Ce^{4+}_{CeO_2}$, and for smaller contributions of Ce^{3+}_{glass}, the residue edge energy became too small to be within 1 eV of the CeO_2 edge energy (e.g., $f_{Pu10S-If} = 0.64$ in Fig. 4). Furthermore, for Ce^{3+}_{glass} contributions larger than 75% (e.g., $f_{Pu10S-If} = 0.80$ in Fig. 4), the residue XANES contained negative values of μ, giving additional support to our determined $f_{Pu10S-If}$ value of 0.72 ± 0.03. Note also that the energies of the various XANES features in the residues do not vary with different contributions of the Pu10S-If sample XANES. This invariance indicates that these features are real.

This analysis has provided two important results. We have independently determined the contribution of the Ce^{4+}_{glass} XANES to the overall Pu10S-IIa Ce XANES to be $28 \pm 3\%$, a value which is within experimental error of that determined chemically ($36 \pm 6\%$). Secondly, we obtained a model XANES spectrum for the Ce^{4+}_{glass} environment, which is presented in Fig. 3 (see above) for comparison with the $Ce^{4+}_{CeO_2}$ XANES. Although the edge energies are the same, the Ce^{4+}_{glass} XANES differs from that of $Ce^{4+}_{CeO_2}$ in several ways. These differences, however, are not unexpected and are accountable based on the current understanding of Ce XANES theory [9,13].

Relative to the intensity of the 5740 eV feature, the feature B_1 at 5727 eV resolved in the XANES of $Ce^{4+}_{CeO_2}$ is less intense in that of Ce^{4+}_{glass}. Also, feature B_2 in the Ce^{4+}_{glass} XANES decreases in intensity and is approximately 1 eV larger in energy than that found in the $Ce^{4+}_{CeO_2}$ XANES. The B_1 and B_2 components of the ≈ 5730 eV region of Ce^{4+} XANES spectra could be due to crystal field effects, but have also been attributed to, respectively, localized (i.e., ionic) and delocalized (i.e., covalent) $M5d^14f^1L$ final states [9]. Differences in the degree of covalent bonding in the Ce–O complexes as well as variations in the long range interactions that influence band structures between the Ce^{4+}_{glass} and $Ce^{4+}_{CeO_2}$ environments are expected [9,13] to produce the observed differences in both the relative intensities and positions of the B_1 and B_2 features between the Ce^{4+}_{glass} and $Ce^{4+}_{CeO_2}$ XANES.

Additionally, the ≈ 5740 eV feature appears to occur at a smaller energy in the Ce^{4+}_{glass} XANES compared to that of the $Ce^{4+}_{CeO_2}$ XANES, which we attribute to a difference in the energies and relative contributions of C_1 and C_2 in the two environments. The splitting of the ≈ 5740 eV feature into C_1 and C_2 is also attributed to crystal field effects [9]. Again, differences in the degree of covalent bonding in the Ce–O complexes between the Ce^{4+}_{glass} and $Ce^{4+}_{CeO_2}$ environments are expected to produce the

[2] Generally, a decrease in the oxidation state of a metal produces a shift in its edge to lower energy (see Refs. [7,14]). Since the bound state feature B_1 does not shift in energy (see Refs. [3,12]) and the main edge energy (as determined by the arctangent used in fitting, see Ref. [10]) varies only by about 1 eV between Ce compounds of the same oxidation state, the maximum variation we would expect in the Ce^{4+} moieties being considered here is ± 1 eV.

observed differences in the energies and relative contributions of the C_1 and C_2 features [9,13], which in turn effect the position of the ≈ 5740 eV XANES peak.

For comparison and for future reference, the extracted Ce^{4+}_{glass} XANES spectrum obtained using the method described here (Fig. 3) was also fitted using one arctangent and five Lorentzian functions. The results of this analysis are summarized in Appendix B.

4.4. Fitting of XANES spectra and cerium speciation

Using weighted contributions from the model XANES spectra of the Ce^{3+}_{glass}, Ce^{4+}_{glass}, and $Ce^{4+}_{CeO_2}$ environments enabled us to fit the experimentally measured XANES spectrum of each glass. The Ce L_{III} XANES experimentally obtained from the Pu10S-II and Pu10S-I series samples along with the fits to the data are depicted in Fig. 5a and b, respectively. The exact contribution from each environment to the overall Ce XANES along with the relative amount of Ce^{4+} with respect to the total Ce content determined by XANES are summarized in Table 4 for each sample composition.

Note the agreement (correlation coefficient, r, of 0.93) between $[Ce^{4+}]/[Ce_{total}]$ values independently determined by the chemical method [11] and those determined by XANES, which gives us confidence in the abilities of both techniques to accurately evaluate the redox chemistry of cerium in these samples. We extrapolate this confidence in XANES analyses to those glasses which contain iron and/or other species that would interfere with chemical analyses.

For the Pu10S-Ia, -Ic, and -Ie samples, prepared by melting at 1120°C for 4 h, the values of $[Ce^{4+}]/[Ce_{total}]$, 0.54 ± 0.05, were all within experimental error. This average value is in agreement with those obtained by Gottardi et al. [18] for related (but different) cerium doped alkali/alkaline earth borosilicate glasses melted at various temperatures for 3 h. Extrapolating from their results for relevant glasses prepared at 1100°C and 1200°C, gave approximate $[Ce^{4+}]/[Ce_{total}]$ values of 0.5.

Fits to the Ce L_{III} XANES of the Pu10S-Ia, -Ic, and -Ie samples (Fig. 5b) required contributions from all three model environments: Ce^{3+}_{glass}, Ce^{4+}_{glass}, and $Ce^{4+}_{CeO_2}$. Crystals of CeO_2 were clearly discernible in

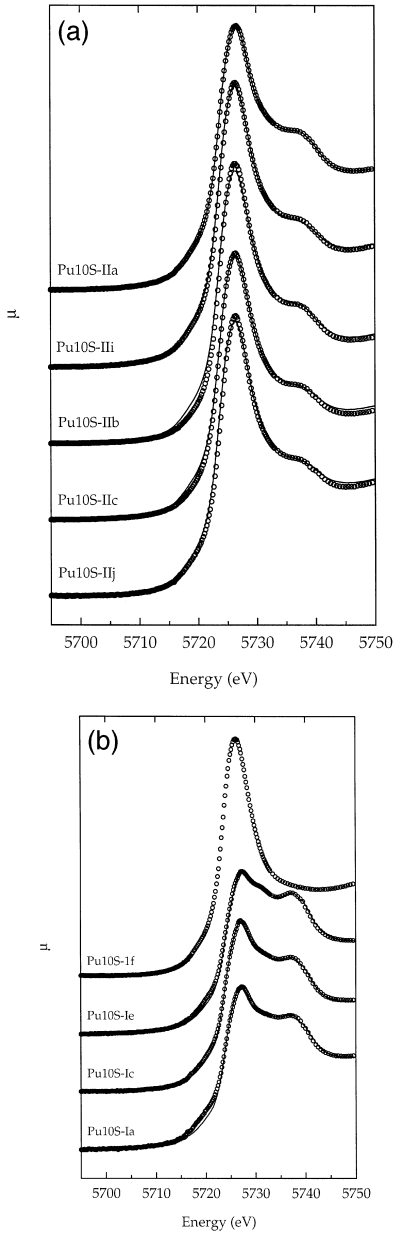

Fig. 5. (a) Cerium L_{III} XANES of all the glasses in the Pu10S-II series. Open circles represent the experimental data while the solid line represents the best fit to the data using the method described here. (b) Cerium L_{III} XANES of all the glasses in the Pu10S-I series. Open circles represent the experimental data while the solid line represents the best fit to the data using the method described here.

a sample of the Pu10S-Ie composition, and were attributed to undissolved CeO_2 particles [11]. On this basis, the need for including a contribution from $Ce^{4+}_{CeO_2}$ XANES to the overall spectrum of this sample (Table 4) is confirmed. Based on a lack of any observable undissolved CeO_2 particles or phase separation, as discussed above, samples from compositions Pu10S-Ia and Pu10S-Ic were assumed to be homogeneous. However, Table 4 indicates that some $Ce^{4+}_{CeO_2}$ is present in these samples, presumably in a form that is beyond the limit of detection by optical microscopy or XRD. For example, since all the glasses studied contained Gd_2O_3 and the Pu10S-I series contained a considerable amount of ZrO_2, it is conceivable that CeO_2–ZrO_2 or Gd_2O_3–CeO_2 solid solution crystals or clusters [19,20] could be present in these samples. Resolving the spectra of separated CeO_2, CeO_2–ZrO_2, and Gd_2O_3–CeO_2 phases using XANES might be difficult considering the similarities in local structural and bonding environments within these series of compounds [19,20].

The $[Ce^{4+}]/[Ce_{total}]$ ratio for the Pu10S-II compositions were less than those for the Pu10S-Ia, -Ic, and -Ie compositions. The differences in both composition and melting temperature (the Pu10S-II compositions were melted at greater temperatures than the Pu10S-I compositions) may have contributed to these differences in the $[Ce^{4+}]/[Ce_{total}]$ ratio [18]. Furthermore, the Ce L_{III} XANES of all of the Pu10S-II samples (Fig. 5a) were fitted using contributions from only the Ce^{3+}_{glass} and Ce^{4+}_{glass} environments. Even for samples with P_2O_5 additions which exhibited opalescence (Pu10S-Ij), only Ce^{3+}_{glass} and Ce^{4+}_{glass} environments were required to fit their XANES spectra.

For the Pu10S-If sample, which was prepared by adding graphite to the batch formulation, chemical analysis indicated that full reduction of the cerium to Ce^{3+} was obtained. This result was confirmed using XANES which also indicated that the cerium was incorporated into the glass as Ce^{3+} (i.e., Ce^{3+}_{glass}).

We can thus use XANES to directly determine the $[Ce^{4+}]/[Ce_{total}]$ ratio in glasses and to determine the distribution of Ce environments, and, in particular, identify the presence of any separated CeO_2 phases. Although these separated phases detected by XANES may be too small to significantly affect the properties of the solid, their detection nevertheless allows us to identify glass systems with a propensity to phase separate or to hinder the dissolution of feed particles at higher concentrations of CeO_2.

5. Conclusion

The experimentally determined XANES spectra of fully reduced Ce^{3+} in one of our glass samples where carbon was used as a reducing agent, of fully oxidized Ce^{4+} in a crystalline CeO_2 reference sample, as well as the XANES spectra of Ce^{4+} in our samples, which was extracted from the experimental data, were used as model XANES for three different Ce chemical and structural environments: respectively, Ce^{3+}_{glass}, $Ce^{4+}_{CeO_2}$, and Ce^{4+}_{glass}. Using weighted contributions from the model XANES spectra of the Ce^{3+}_{glass}, Ce^{4+}_{glass}, and $Ce^{4+}_{CeO_2}$ environments, the experimentally measured XANES spectrum of each sample was fitted. Thus, the $[Ce^{4+}]/[Ce_{total}]$ ratio and the distribution of Ce environments were determined for each glass. The Ce L_{III} XANES of all of the Pu10S-II samples, which exhibited $[Ce^{4+}]/[Ce_{total}]$ ratios in the range 0.15 to 0.28 (determined from the XANES results), were fitted using contributions from only the Ce^{3+}_{glass} and Ce^{4+}_{glass} environments. Fits to the XANES of non-reduced Pu10S-I samples, which exhibited $[Ce^{4+}]/[Ce_{total}]$ ratios in the range 0.51 to 0.58, required an additional contribution from the $Ce^{4+}_{CeO_2}$ environment, indicating that CeO_2-based phase separation had occurred in these glasses. All of the $[Ce^{4+}]/[Ce_{total}]$ ratios determined by XANES spectroscopy correlated, $r > 0.9$, with those independently obtained using wet chemical methods.

Acknowledgements

This work was supported by the U.S. Department of Energy under contract DE-AC06-76RLO 1830. The authors would like to thank the experimental assistance of our co-workers at the Pacific Northwest National Laboratory: D. McCready and J. Young. H. Li is grateful to Associated Western Universities, for his postdoctoral appointment at the Pacific Northwest National Laboratory during the time when this work was performed. We acknowledge the use of beam line X19A at the National Synchrotron Light

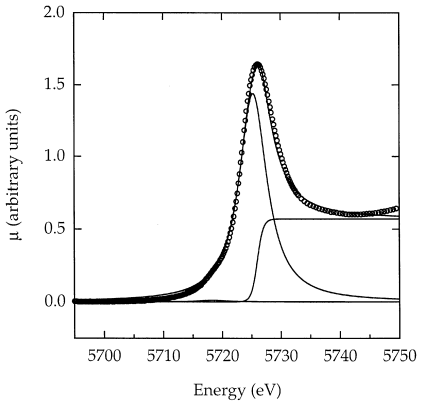

Fig. 6. Cerium L_{III} XANES obtained from the Pu10S-If glass (open circles) and the best fit to the data using one arctangent function and two Lorentzian (A and B_1) functions (solid lines).

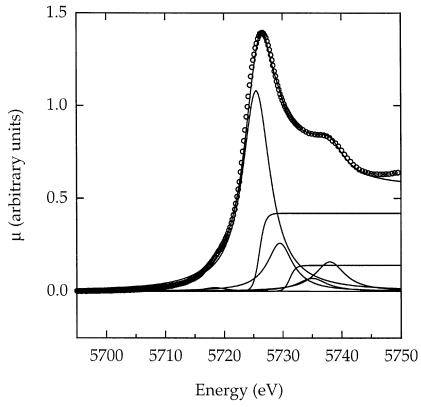

Fig. 8. Cerium L_{III} XANES obtained from the Pu10S-IIa glass (open circles) and the best fit to the data using two arctangent functions and five Lorentzian functions (solid lines).

Source at Brookhaven National Laboratory (operated by the U.S. Department of Energy) and the assistance of beam line spokesperson L. Fürenlid. The authors would also like to acknowledge the helpful comments received from the reviews and editor of this manuscript.

Appendix A

The experimental Ce L_{III} XANES spectrum of the Pu10S-If sample was fitted (Fig. 6) using one arctangent function as well as two Lorentzian functions corresponding to the A and B_1 features. The XANES obtained from the CeO_2 reference material was fitted (Fig. 7) in a similar manner, but with additional contributions of three more Lorentzian functions, designated B_2, C_1, and C_2.

The fitting of the Ce L_{III} XANES spectra of the Pu10S-IIa and -Ic samples (Figs. 8 and 9) were more complicated since we knew from chemical analyses that both Ce^{3+} and Ce^{4+} were present in the samples. We also knew from XRD that CeO_2 was present in a Pu10S-Ic sample. Two arctangent functions and up to seven Lorentzian functions were thus used to fit the XANES spectra obtained from these samples.

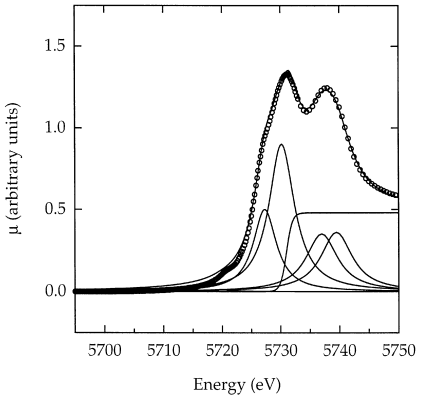

Fig. 7. Cerium L_{III} XANES obtained from the CeO_2 reference material (open circles) and the best fit to the data using one arctangent function and five Lorentzian (A, B_1, B_2, C_1, and C_2) functions (solid lines).

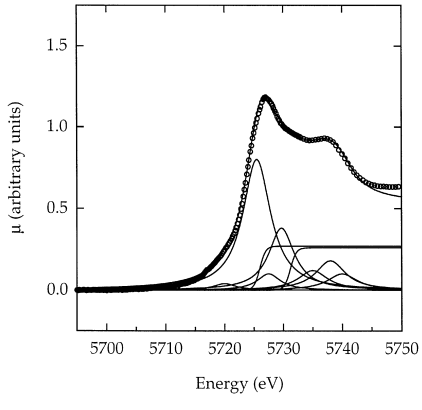

Fig. 9. Cerium L_{III} XANES obtained from the Pu10S-Ic glass (open circles) and the best fit to the data using two arctangent functions and seven Lorentzian functions (solid lines).

Table 5
The energy position (E, ± 0.1 eV), width (W, ± 0.1 eV), and amplitude (H, ± 0.01) of each arctangent and Lorentzian function used to fit the Ce L_{III} XANES spectra of the Pu10S-If glass, CeO_2, and the Pu10S-IIa and -Ic glasses

Sample	Arctangent parameters				Lorentzian parameters			
	E (eV)	W (eV)	H	Feature	E (eV)	W (eV)	H	Feature
Pu10S-If	5726.0	1.2	0.57	III_{glass}	5718.4	2.9	0.01	A
					5725.3	2.9	1.44	B_1
CeO_2	5731.0	1.2	0.50	$IVCeO_2$	5720.0	2.4	0.02	A
					5727.3	2.4	0.50	B_1
					5730.2	2.6	0.90	B_2
					5737.0	3.0	0.35	C_1
					5739.5	2.9	0.36	C_2
Pu10S-IIa	5726.0	1.2	0.42	III_{glass}	5718.4	2.4	0.02	A^a
					5725.5	2.9	1.08	B_1^b
	5731.2	1.2	0.14	IV_{glass}	5729.5	2.6	0.26	B_2^c
					5735.0	3.0	0.07	C_1
					5738.0	3.0	0.16	C_2
Pu10A-Ic	5726.0	1.2	0.27	III_{glass}	5725.5	2.9	0.80	B_1^b
	5731.2	1.2	0.26	IV^d	5720.0	2.4	0.04	A^e
					5727.5	2.4	0.10	B_1^d
					5729.9	2.6	0.38	B_2^d
					5735.0	3.0	0.12	C^f
					5738.0	3.0	0.18	C^f
					5740.0	3.0	0.10	C^f

[a]Although glass Pu10S-IIa contained both Ce^{3+} and Ce^{4+}, only one A-feature Lorentzian (corresponding to Ce^{3+}) was used in the fitting procedure.

[b]The position of the B_1-feature Lorentzian function that gave the best fit to the XANES of the Pu10S-IIa and -Ic glasses (5725.5 eV) most closely resembled that of the Ce^{3+} environment (5725.3 eV) but was slightly higher in energy, probably the result of unaccounted Ce^{4+} B_1 Lorentzian contributions.

[c]The position of the B_2-feature Lorentzian function that gave the best fit to the XANES of the Pu10S-IIa glass (5729.5 eV) most closely resembled that of the Ce^{4+} environment (5730.2 eV) but was slightly lower in energy, probably the result of an unaccounted Ce^{4+} B_1 Lorentzian contribution.

[d]The energy position of the arctangent function used to fit the Pu10S-Ic glass was slightly different from that used to fit CeO_2 and is most likely due to the presence of multiple Ce^{4+} environments. The positions of the B_1- and B_2-feature Lorentzian functions that gave the best fit to the XANES of this glass (5727.5 eV and 5729.9 eV, respectively) closely resembled those of the $Ce^{4+}_{CeO_2}$ environment (5727.3 eV and 5730.2 eV) as well as those of the Ce^{4+}_{glass} environment (5727.3 eV and 5729.7 eV, see Appendix B).

[e]Although glass Pu10S-Ic contained both Ce^{3+} and Ce^{4+}, only one A-feature Lorentzian (corresponding to Ce^{4+}) was used in the fitting procedure.

[f]More than two C-feature Lorentzians were required to fit the XANES of the Pu10S-Ic glass, again indicating that multiple Ce^{4+} environments were present in this glass (see Appendix B).

Table 6
Arctangent (III_{glass} and IV_{glass}) and Lorentzian (A, B_1, B_2, C_1, and C_2) function amplitudes (± 0.01) used to fit the Pu10S-IIb, -IIc, -IIi, and -IIj glasses

Sample	Function						
	III_{glass}	IV_{glass}	A	B_1	B_2	C_1	C_2
Pu10S-IIa	0.42	0.14	0.02	1.08	0.26	0.07	0.16
Pu10S-IIb	0.43	0.08	0.01	1.20	0.14	0.05	0.10
Pu10S-IIc	0.43	0.08	0.01	1.16	0.12	0.05	0.10
Pu10S-IIi	0.47	0.10	0.01	1.21	0.15	0.05	0.10
Pu10S-IIj	0.46	0.07	0.01	1.21	0.13	0.04	0.08

The energy positions and widths for the fitting functions were fixed at the same values for those used to fit the Ce L_{III} XANES of the Pu10S-IIa glass (Table 5).

The energy, width, and amplitude (height) of each arctangent and Lorentzian function used to fit the Ce L_{III} XANES spectra of CeO_2 and of the Pu10S-If, -IIa, and -Ic samples are summarized in Table 5.

Using the same energies and widths for the arctangent and Lorentzian functions used to fit the Ce L_{III} XANES of the Pu10S-IIa glass, the XANES of the Pu10S-IIb, -IIc, -IIi, and -IIj samples were fitted by adjusting the relative function amplitudes. These results are summarized in Table 6.

Finally, Table 7 compares the relative amount of Ce^{4+} with respect to Ce_{total} determined by chemical analysis to the relative area of the C_1 and C_2 Lorentzians (A_C) with respect to the total Lorentzian peak area (A_{A+B+C}). By using the method of fitting the Ce L_{III} XANES data with a series of arctangent and Lorentzian functions, the combined relative area of the C peaks is the only unique feature that can be

Table 7
Comparison between the relative amounts of Ce^{4+} with respect to Ce_{total} determined by chemical analysis and the relative area of the C_1 and C_2 Lorentzians (A_C) with respect to the total Lorentzian peak area (A_{A+B+C})

Sample	Ce^{4+} (% w/r Ce_{total})	A_C (% w/r A_{A+B+C})
Pu10S-If	0	0
Pu10S-IIj	24 ± 4	5.0 ± 0.5
Pu10S-IIc	25 ± 4	6.2 ± 0.6
Pu10S-IIi	25 ± 4	6.1 ± 0.6
Pu10S-IIb	29 ± 4	6.1 ± 0.6
Pu10S-IIa	36 ± 5	9.1 ± 0.9
Pu10S-Ic	47 ± 6	15 ± 2

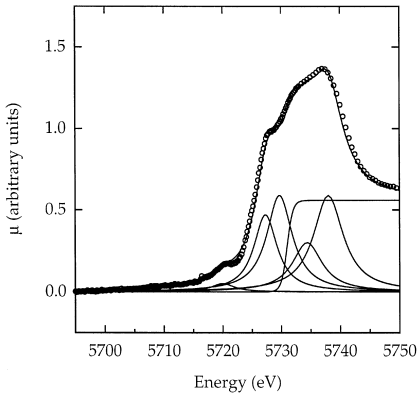

Fig. 10. Extracted Ce L_{III} XANES of the Ce^{4+}_{glass} environment, see main text, (open circles) and the best fit to the data using one arctangent functions and five Lorentzian functions (solid lines).

used to quantify the relative amount Ce^{4+} species, provided that the results are calibrated against independently determined values of $[Ce^{4+}]/[Ce_{total}]$. The results presented in Table 7 should thus be useful in this regard.

Appendix B

The extracted Ce^{4+}_{glass} XANES spectrum obtained using the more novel approach described in the main text of this article was fitted (Fig. 10) using one arctangent functions and five Lorentzian functions. The energy position, width, and amplitude (height) of each function used to fit this XANES spectrum are summarized in Table 8. Note that these fitting parameters differ from those used to fit the CeO_2 spectrum.

Table 8
The energy position (E, ± 0.1 eV), width (W, ± 0.1 eV), and amplitude (H, ± 0.01) of each arctangent and Lorentzian function used to fit the extracted Ce L_{III} XANES of the Ce^{4+}_{glass} environment

Environment	Arctangent parameters				Lorentzian parameters			
	E (eV)	W (eV)	H	Feature	E (eV)	W (eV)	H	Feature
Ce^{4+}_{glass}	5731.0	1.2	0.56	IV_{glass}	5720.0	2.4	0.05	A
					5727.3	2.4	0.47	B_1
					5729.7	2.6	0.59	B_2
					5734.4	3.0	0.30	C_1
					5738.0	2.9	0.59	C_2

References

[1] B.T. Kilbourn, Cerium: A Guide to Its Role in Chemical Technology, Molycorp, White Plains, NY, 1992, pp. 26–28.
[2] A. Paul, Phys. Chem. Glasses 17 (1976) 7.
[3] D.L. Blanchard, D.S. Sunberg, R.A. Craig, M. Bliss, M.J. Weber, in: Stanford Synchrotron Radiation Laboratory 1994 Activity Report, Stanford, CA, 1994, pp. 188–191.
[4] E.R. Vance, K.P. Hart, R.A. Day, B.D. Begg, P.J. Angel, E. Loi, J. Weir, V.M. Oversby, in: Scientific Basis for Nuclear Waste Management XIX, Materials Research Society Symposium Proceedings, Vol. 412, Materials Research Society, Pittsburgh, PA, 1996, pp. 49–55.
[5] S.A. Dmitriev, S.V. Stefanovsky, in: Scientific Basis for Nuclear Waste Management XIX, Materials Research Society Symposium Proceedings, Vol. 412, Materials Research Society, Pittsburgh, PA, 1996, pp. 239–242.
[6] A. Paul, R.W. Douglas, Phys. Chem. Glasses 6 (1965) 212.
[7] G.E. Brown, G. Calas, G.A. Waychunas, J. Petiau, in: F.C. Hawthorne (Ed.), Spectroscopic Methods in Mineralogy and Geology, Reviews in Mineralogy, Vol. 18, Mineralogical Society of America, Washington, DC, 1988, pp. 431–512.
[8] H. Li, J.G. Darab, D.W. Matson, P.A. Smith, P. Hrma, Y. Chen, J. Liu, in: Scientific Basis for Nuclear Waste Management XIX Materials Research Society, Pittsburgh, PA, 1996, pp. 141–148.
[9] F. Le Normand, L. Hilaire, K. Kili, G. Krill, G. Maire, J. Phys. Chem. 92 (1988) 2561.
[10] J.E. Sunstrom, S.M. Kauzlarich, M.R. Antonio, Chem. Mater. 5 (1993) 182.
[11] H. Li, J.D. Vienna, P. Hrma, M.J. Schweiger, D.E. Smith, M. Gong, in: Ceramic Transactions, American Ceramic Society, Westerville, OH, in press.
[12] M.R. Antonio, J.S. Xue, L. Soderholm, J. Alloys Compounds 207–208 (1994) 444.
[13] A. Bianconi, A. Marceli, H. Dexpert, R. Karnatak, A. Kotani, T. Jo, J. Petiau, Phys. Rev. B 35 (1987) 806.
[14] R.K. MacCrone, J.G. Darab, in: L.D. Pye, W.C. LaCourse, H.J. Stevens (Eds.), The Physics of Non-Crystalline Solids, Taylor and Francis, Washington DC, 1992, pp. 724–730.
[15] J.G. Darab, H. Li, D.W. Matson, P.A. Smith, in: K.L. D'Amico, L.J. Terminello, D.K. Shuh (Eds.), Synchrotron Radiation Techniques in Industrial, Chemical, and Materials Science, Plenum, New York, 1996, pp. 237–255.
[16] F.A. Cotton, G. Wilkinson, in: Advanced Inorganic Chemistry, 4th edn., Wiley, New York, 1980, pp. 999–1046.
[17] F.A. Cotton, G. Wilkinson, in: K.L. D'Amico, L.J. Terminello, D.K. Shuh (Eds.), Synchrotron Radiation Techniques in Industrial, Chemical, and Materials Science, Plenum, New York, 1996, pp. 824–831.
[18] V. Gottardi, G. Paoletti, M. Tornati, in: Advances in Glass Technology, Plenum, New York, 1962, pp. 412–423.
[19] P. Li, W-I. Chen, J.E. Penner-Hahn, T.-Y. Tien, J. Am. Ceram. Soc. 74 (1991) 958.
[20] P. Li, I-W. Chen, J.E. Penner-Hahn, Phys. Rev. B (1993) 10063.